## Characterizing Anomalous High-Harmonic Generation in Solids

Lun Yue<sup>®</sup> and Mette B. Gaarde<sup>®†</sup>

Department of Physics and Astronomy, Louisiana State University, Baton Rouge, Louisiana 70803-4001, USA

(Received 23 June 2022; revised 30 December 2022; accepted 28 March 2023; published 21 April 2023)

Anomalous high-harmonic generation (HHG) arises in certain solids when irradiated by an intense laser field, originating from a Berry-curvature-induced perpendicular anomalous current. The observation of pure anomalous harmonics is, however, often prohibited by contamination from harmonics stemming from interband coherences. Here, we fully characterize the anomalous HHG mechanism, via development of an ab initio methodology for strong-field laser-solid interaction that allows a rigorous decomposition of the total current. We identify two unique properties of the anomalous harmonic yields: an overall yield increase with laser wavelength; and pronounced minima at certain laser wavelengths and laser intensities around which the spectral phases drastically change. Such signatures can be exploited to disentangle the anomalous harmonics from competing HHG mechanisms, and thus pave the way for the experimental identification and time-domain control of pure anomalous harmonics, as well as reconstruction of Berry curvatures.

DOI: 10.1103/PhysRevLett.130.166903

When a charge carrier in a crystal with a nonvanishing Berry curvature is perturbed by a weak electric field, it acquires an anomalous perpendicular velocity component [1-5] and a corresponding anomalous current. Such anomalous velocities and Berry curvatures are ubiquitous in modern physics and are, e.g., responsible for various Hall effects [6,7]. With the advancements in light-source technologies [8,9] and the availability of intense laser pulses, it is now possible to induce highly nonperturbative anomalous currents that are sources for anomalous highharmonic generation (HHG) [10-14]. The broadening of our understanding of the anomalous current from the conventional low-energy condensed-matter physics to the extreme nonperturbative regime [15-18] is of utmost importance for both fundamental and application purposes.

In the strong-field regime, it is a challenge to extract detailed information from experiment and theory, given the multitude of nonperturbative phenomena that are driven simultaneously in a material. Such a situation is sketched in Fig. 1, in which a linearly polarized laser field induces two perpendicular currents: an anomalous current and an interband current [19]. An open question is which of these contributions dominate, a subject that has been under contention in recent interpretations of HHG experiments: the measured perpendicular-polarized harmonics have been attributed entirely to either Berry curvatures [10–12,14] or interband coherences [20-24]. Similarly, no theoretical studies on the nonperturbative anomalous current have fully characterized its competition with the other generation mechanisms [25-27]. A theoretical framework that can facilitate the rigorous isolation of the anomalous HHG, and provide signatures and guidelines for their experimental identification is highly desired.

The generation and identification of pure anomalous currents and high harmonics are, besides the fundamental aspects, also relevant for application and spectroscopy purposes. It is well known that different generation mechanisms exhibit distinct characteristics in the spectral and temporal domains, where, e.g., distinct subcycle emission features had previously aided experiments in determining the underlying HHG mechanisms in quartz as intraband [28,29], and in ZnO as interband [30,31]. Determining similar characteristics for anomalous HHG would aid in the understanding of phase-matching conditions for the development of new light sources [16,29,32], as well as the optical control of electronic currents at the petahertz rates [28,33–36]. Additionally, generating pure anomalous harmonics is a prerequisite for Berry-curvature high-harmonic spectroscopy [11,14], which adds to the already burgeoning field of high-harmonic spectroscopy [12,13,28–31,37–49].

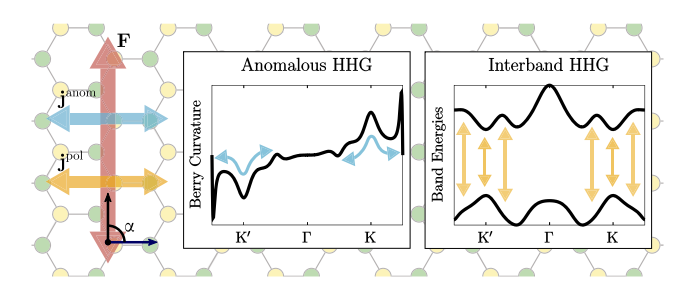


FIG. 1. In a crystal, a strong laser field  $\mathbf{F}(t)$ , polarized at an angle  $\alpha$  relative to the mirror axis of a hexagonal crystal, induces nonperturbative perpendicular currents  $\mathbf{j}^{\text{anom}}(t)$  and  $\mathbf{j}^{\text{pol}}(t)$  that are sources for anomalous and interband HHG. The insets sketch the underlying generation mechanisms.

In this Letter, we characterize the unique properties of the anomalous HHG current, allowing us to distinguish it from the other contributions through its intensity and wavelength dependence as well as its subcycle emission dynamics. For this purpose, we develop an ab initio methodology for strong-field light-matter interaction that allows a rigorous decomposition of the total current into its Bloch-gauge-invariant constituents, without the explicit need for the construction of a globally smooth and periodic Bloch gauge [7,50–55]. We consider monolayer MoS<sub>2</sub> as our specific target system for HHG, due to its potential technological applications [56-58] and the absence of propagation effects. We identify two main signatures of the anomalous harmonics: (i) a yield increase with laser wavelength and dominance over the interband harmonics below a threshold harmonic energy; (ii) characteristic minima in the yield for certain laser wavelengths or intensities around which the subcycle time structure drastically changes. We employ a semiclassical model to extract the underlying physics, whereby signature (ii) is traced to a  $\pi$  jump of the harmonic spectral phase. Our results add to the fundamental understanding of nonperturbative anomalous currents, provide a guide towards experimental identification and control of pure anomalous harmonics, and resolve an open debate on the origin of perpendicularpolarized high harmonics in solids [10–12,14,20–24].

Our *ab initio* methodology starts with the calculation of the monolayer  $\text{MoS}_2$  band structure  $E_n^{\mathbf{k}}$  and momentum coupling matrix elements  $\mathbf{p}_{mn}^{\mathbf{k}}$ , employing density functional theory [59] with ONCV pseudopotentials [60,61] and PBE functionals [62]. Atomic units are used throughout this Letter unless indicated otherwise. The Brillouin zone is sampled with N=8100 points in a Monkhorst-Pack mesh. For the dynamics, we solve the time-dependent equations for the density matrix elements  $\rho_{mn}^{\mathbf{k}}(t)$  in the velocity gauge [53,55,63], taking into account 90 bands. At every 5th step of the time propagation, we transform into an adiabatic basis [55] to include a dephasing time  $T_2=10$  fs, and decompose the total current into four Bloch-gauge-invariant terms,  $\mathbf{j}(t)=\mathbf{j}^{\text{tra}}(t)+\mathbf{j}^{\text{pol}}(t)+\mathbf{j}^{\text{anom}}(t)+\mathbf{j}^{\text{mix}}(t)$ , where

$$\mathbf{j}^{\text{tra}}(t) = -N^{-1} \sum_{n\mathbf{k}} \tilde{\mathbf{p}}_{nn}^{\mathbf{k}}(t) \tilde{\rho}_{nn}^{\mathbf{k}}(t), \tag{1a}$$

$$\mathbf{j}^{\text{pol}}(t) = -N^{-1} \partial_t \sum_{m \neq n, \mathbf{k}} \tilde{\mathbf{d}}_{mn}^{\mathbf{k}}(t) \tilde{\rho}_{nm}^{\mathbf{k}}(t), \tag{1b}$$

$$\mathbf{j}^{\text{anom}}(t) = -N^{-1} \sum_{n\mathbf{k}} [\mathbf{F}(t) \times \tilde{\mathbf{\Omega}}_{n}^{\mathbf{k}}(t)] \tilde{\rho}_{nn}^{\mathbf{k}}(t), \tag{1c}$$

$$\mathbf{j}^{\mathrm{mix}}(t) = -N^{-1} \sum_{\mu=x,y} F_{\mu}(t) \sum_{m \neq n,\mathbf{k}} [\tilde{d}^{\mathbf{k}}_{\mu,mn}(t)]_{;\mathbf{k}} \tilde{\rho}^{\mathbf{k}}_{nm}(t), \qquad (1\mathrm{d})$$

with  $\mathbf{j}^{\text{tra}}(t)$  the intraband current,  $\mathbf{j}^{\text{pol}}(t)$  the interband (polarization) current,  $\mathbf{j}^{\text{anom}}(t)$  the anomalous current,

and  $\mathbf{j}^{\text{mix}}(t)$  the mixture current originating in the coupling between the intraband and interband position operators [27,55,67,68]. The tildes in Eq. (1) indicate quantities evaluated in the adiabatic basis. After calculation of the current decomposition at time t, we transform back into the Bloch basis and continue with the time-dependent propagation of  $\rho_{mn}^{\bf k}(t)$ . We evaluate the dipole matrix elements  $\tilde{\bf d}_{mn}^{\bf k}(t)$ , generalized gradients  $[\tilde{d}_{\mu,mn}^{\bf k}(t)]_{;\bf k}$  [68,69], and Berry curvatures  $\tilde{\Omega}_n^{\mathbf{k}}(t)$  entirely in terms of  $\tilde{E}_n^{\mathbf{k}}(t)$  and  $\tilde{\mathbf{p}}_{mn}^{\mathbf{k}}(t)$  by using relevant sum-rules [68–70]. The key advantage of this methodology is that it does not require the construction of a globally smooth and periodic gauge for the Bloch states, in contrast to previous methods that decompose the current [27,68,71], but instead requires more bands for convergence (see Supplemental Material [63]). The electric field,  $\mathbf{F}(t) = -\partial_t \mathbf{A}(t)$ , is linearly polarized in the plane of the monolayer, and the vector potential  $\mathbf{A}(t)$  has a total duration of 12 optical cycles and a  $\cos^2$ envelope. Since  $\mathbf{j}^{\text{anom}}(t) \perp \mathbf{F}(t)$ , we focus our attention on the harmonic spectra polarized perpendicular to the laser field,  $S(\omega) = \omega^2 |\mathbf{j}(\omega) \cdot \hat{\mathbf{e}}_{\perp}|^2$ , with  $\mathbf{j}(\omega) = \int_{-\infty}^{\infty} dt e^{i\omega t} \mathbf{j}(t)$ . Note that excitonic effects have been neglected in this Letter. Although this is appropriate for the system and regime we are in according to [15,63], it is an ongoing effort in the community to understand excitonic effects on HHG [72,73].

We highlight that we do not label the anomalous current as an intraband contribution: even though  $\mathbf{j}^{\text{anom}}(t)$  in Eq. (1c) does not depend on the time-dependent coherences, the Berry curvature for the *n*th band arises from the residual coupling between the other bands [6,63,70]. In addition, it can be easily shown that the oft-used expression for the "interband" current  $N^{-1} \sum_{m \neq n, \mathbf{k}} \tilde{\mathbf{p}}_{mn}^{\mathbf{k}}(t) \tilde{\rho}_{nm}^{\mathbf{k}}(t)$ equals  $\mathbf{j}^{\text{pol}}(t) + \mathbf{j}^{\text{anom}}(t) + \mathbf{j}^{\text{mix}}(t)$ . In this sense, the experimentally measured perpendicular harmonics interpreted as interband [20-24] likely already contains the anomalous contribution, while in this Letter, interband current refers to  $\mathbf{i}^{\text{pol}}(t)$  of Eq. (1b) [74]. Considering  $\mathbf{i}^{\text{anom}}(t)$  as a standalone contribution to the total current facilitates a link between the weak-field condensed matter community, where Berry curvatures and anomalous velocities are ubiquitous, and the strong-field community. As we will see, the anomalous high harmonics exhibit unique characteristics separating them from other HHG contributions.

Figure 2(a) shows the decomposed perpendicular-polarized harmonic spectrum for a field with carrier wavelength 7.4  $\mu$ m, intensity 50 GW/cm², and  $\alpha = 30^{\circ}$  ( $\alpha$  defined in Fig. 1). Only even-order harmonics are observed, with the interband and anomalous contributions clearly competing: the interband harmonics dominate at higher orders, even well below the band gap energy at around harmonic 8 (H8) and H10; while the anomalous harmonics dominate for the lowest orders at H2–H6. The intraband and mixture currents contribute with yields that are order(s) of magnitude lower.

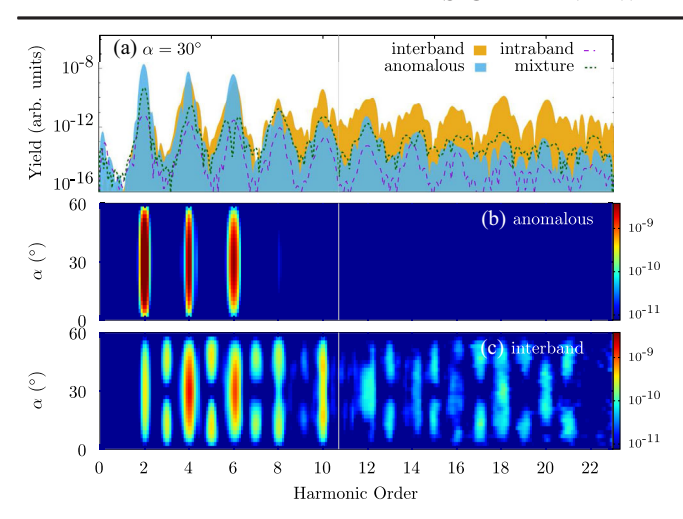


FIG. 2. Spectra for perpendicular-polarized harmonics in monolayer  $MoS_2$  for a 7.4  $\mu m$  driver. (a) Different current-contributions to spectrum for  $\alpha=30^\circ$ . The (b) anomalous and (c) interband harmonics versus  $\alpha$ . The gray vertical lines mark the gap energy.

Figures 2(b) and 2(c) show, respectively, the anomalous and interband HHG spectra versus  $\alpha$ . Our results conform with the dynamical-symmetry selection rules for HHG [75], where the  $D_{3h}$  spatial point group of monolayer MoS<sub>2</sub> together with the in-plane linearly polarized field prohibit the emission of all perpendicular harmonics at  $\alpha = n60^{\circ}$  and odd-order harmonics at  $\alpha = 30^{\circ} + n60^{\circ}$ , with n an integer [10,75–77]. The anomalous harmonics in Fig. 2(b) only permit even orders for all  $\alpha$ , since time-reversal symmetry dictates  $\Omega_m^{-\mathbf{k}} = -\Omega_m^{\mathbf{k}}$  which leads to  $\mathbf{j}^{\text{anom}}[t+(T/2)] = \mathbf{j}^{\text{anom}}(t)$ , with T the optical period. In Fig. 2(c), no symmetry rule prohibits the emission of interband harmonics between  $\alpha = 0^{\circ}$  and  $\alpha = 30^{\circ}$ , and both even and odd orders are observed.

To further characterize the anomalous HHG mechanism and its competition with the other generation mechanisms, we show in Fig. 3 the decomposed harmonic yields for H2-H12 versus laser wavelength, fixing the laser intensity at 50 GW/cm<sup>2</sup> and  $\alpha = 30^{\circ}$ . We focus on the anomalous and interband contributions, which are seen to dominate over the intraband and mixture contributions for almost all wavelengths. At shorter laser wavelengths, in the gray shaded regions of Fig. 3 where the harmonic energy is greater than the gap energy of 1.79 eV, the interband yield dominates over the anomalous yield for all harmonic orders. With increasing wavelength, the anomalous harmonic yield overall increases, and begins to dominate over the interband yield at around a harmonic energy of  $E_h = 1$  eV (marked by purple ticks on the wavelength axis). At the longest wavelength in the figure, 19 µm, the anomalous harmonics dominate completely-e.g., the anomalous H6 yield at 19 µm is around 3 orders of magnitudes greater than the interband yield. We judge the transition energy  $E_h$  to be material dependent and

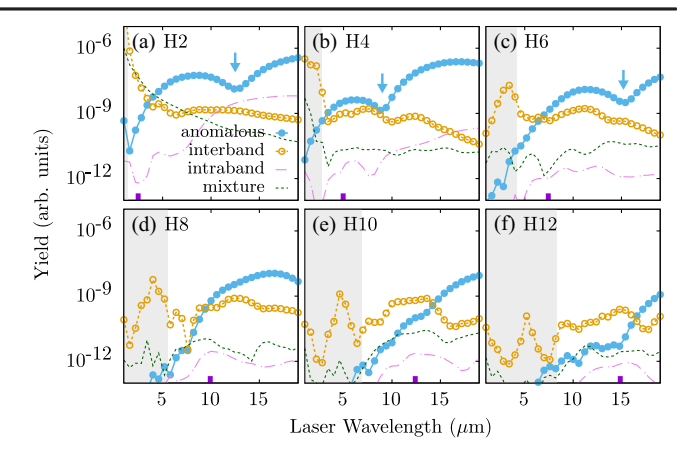


FIG. 3. Decomposed harmonic yields versus laser wavelength for  $\alpha=30^\circ$  and the even harmonic orders H2-H10 [panels (a)–(f)]. The arrows in (a)–(c) mark pronounced minima in the anomalous harmonic yield. In each panel, the gray shaded areas indicate that the harmonic energy is larger than the band gap. Purple ticks on the wavelength axis mark the harmonic energy 1 eV.

governed by the particular band structure and coupling matrix elements of the system, but nonetheless expect it to be generally smaller than the gap energy, as above-bandgap harmonics generally proceeds via interband coherences [74,78]. Figure 3 clears up the recent contention on the origin of the perpendicular harmonics in  $MoS_2$  in terms of either anomalous [10,79,80] or interband harmonics [21–24,79,80]: these two harmonic contributions dominate in different laser-parameter and harmonic-energy regimes.

In Figs. 3(a)–3(c), the anomalous harmonic yield for H2, H4, and H6 exhibit prominent minima marked by blue arrows at 12.5, 9, and 15.2 μm, respectively. We performed additional HHG simulations using a fixed laser wavelength of 7.4 μm and varying laser intensities, and observed similar pronounced minima at specific intensities (see Supplemental Material [63]). These minima represent a striking characteristic of the anomalous harmonics, which we now characterize employing a semiclassical model.

We write the semiclassical anomalous current as  $\mathbf{j}^{\mathrm{SC}}(t) \propto -\mathbf{F}(t) \times [\Delta \mathbf{\Omega}^{\mathrm{K}+\mathbf{A}(t)} + \Delta \mathbf{\Omega}^{\mathrm{K}'+\mathbf{A}(t)}]$ , in which we assume that the electrons tunnel at the minimum band gaps at K and K' [10,81], and adopt a two-band approximation, such that  $\Delta \mathbf{\Omega}^{\mathbf{k}}$  is the Berry curvature difference between the lowest CB and the highest VB, representing the total contribution from the electron and hole. The solid line in Fig. 4(a) shows the z component of  $\Delta \mathbf{\Omega}^{\mathbf{k}}$  along K'- $\Gamma$ -K. The calculated semiclassical yields, using the same laser fields as in the ab initio calculations of Fig. 3, are plotted in Fig. 4(b) for H4 and H6 in solid lines. Clear minima are observed, with the most pronounced minimum seen at  $\sim$ 9  $\mu$ m for H4 and at  $\sim$ 15.7  $\mu$ m for H6, consistent with our ab initio results in Fig. 3. To gain further insight, we assume a monochromatic vector potential  $\mathbf{A}(t) = F_0/\omega_0 \sin(\omega_0 t)\hat{\mathbf{e}}$ , which leads

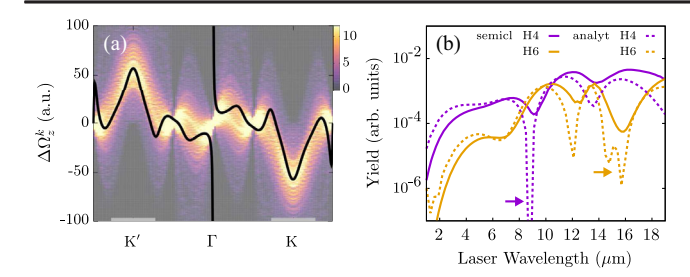


FIG. 4. (a) Berry curvatures: calculated from first principles (solid line); reconstructed from the HHG spectrum in Fig. 2(b) (color plot), with the gray lines marking the excursion regions of electrons and holes created at K and K'. (b) Semiclassical numerical and analytical results (see text) for the anomalous H4 and H6 yields versus wavelength.

to the analytical expression for the current,  $\mathbf{j}^{SC}(t) \propto \sum_{s=1}^{\infty} C_{2s} \sin(2s\omega_0 t)$ , with

$$C_{2s} = \frac{s\omega_0}{a} \sum_{q=1}^{\infty} \frac{\Omega_q}{q} \cos\left(\frac{2q\pi}{3}\right) J_{2s}\left(\frac{qaF_0}{2\omega_0}\right)$$
 (2)

the amplitudes,  $\Omega_q$  the Fourier coefficients of  $\Delta\Omega_z^{\mathbf{k}}$ ,  $J_{2s}$  the (2s)th-order Bessel function, and a the lattice constant. The yield versus wavelength for the (2s)th anomalous harmonic,  $S_{2s} \propto s^2 \omega_0^2 |C_{2s}|^2$ , is plotted in Fig. 4(b) for 2s = 4 and 2s = 6 in dashed lines. The pronounced minima marked by the arrows hence correspond to nodes of  $C_{2s}$  seen as a function of wavelength. We see that the expression for  $C_{2s}$  in Eq. (2) involves both the nonlinearities of the Bessel functions and the Berry curvature Fourier coefficients  $\Omega_a$ . We have checked that the q sum in Eq. (2) is not dominated by a single term, but rather a superposition of terms. In addition, the pronounced minima in the yield-versus-laserintensity plots from the ab initio calculations are also explained in terms of the nodes of  $C_{2s}$  (considered as a function of the laser intensity) [63]. The nodes in  $C_{2s}$  is another characterization tool for the anomalous harmonics, as the presence of such minima in a wavelength or intensity scan is an indication of the dominance of the anomalous HHG mechanism.

Finally, we consider the emission-time profiles and the spectral phases of the solid-state harmonics, which encode pertinent information about the underlying harmonic emission mechanisms [28–31]. In Figs. 5(a) and 5(b), we show the time-frequency profiles for the anomalous harmonic emissions obtained from the *ab initio* calculations, at laser wavelengths corresponding to before and after the H4 minimum at  $\lambda_{\min} \equiv 9$  µm [Fig. 3(b)], respectively. For the 7.6 µm case in Fig. 5(a), the spectral yields around H6 is emitted at t = T/2, corresponding to the electric field extrema, while H4 is emitted at  $t = (n + \frac{1}{2})T/2$  at the zeros of the field. For the longer laser wavelength 10 µm >  $\lambda_{\min}$  in Fig. 5(b), the emission time of H4 and H6 are shifted by a quarter optical cycle.

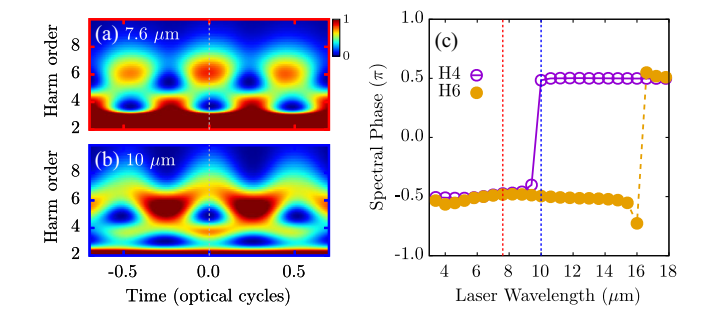


FIG. 5. Time-frequency emission profiles for the anomalous harmonics extracted from the *ab initio* simulations for laser wavelength (a) 7.6 and (b) 10  $\mu$ m. The color bar axis is in linear scale and arbitrary units, and the dashed vertical line is to guide the eyes. (c) Spectral phases for the anomalous H4 and H6 extracted from the simulations, with the wavelengths used in (a) and (b) marked by vertical lines.

These shifts of the anomalous harmonic emission times can be understood in terms of the semiclassical analytical model for the anomalous current. As we have seen, the yield minima of the (2s)th harmonic is explained by the nodes of  $C_{2s}$ . When going through such a node, the real-valued amplitude  $C_{2s}$  changes sign, corresponding to a  $\pi$ -phase shift, which in turn will change the emission-time profiles. We confirm our interpretation by extracting the spectral phases of the anomalous harmonics from our ab initio simulations,  $\varphi^{\text{anom}}(\omega) =$  $\arg[\mathbf{j}^{\text{anom}}(\omega) \cdot \hat{\mathbf{e}}_{\perp}]$ , and present the results in Fig. 5(c). The spectral phases for H4 and H6 for the laser wavelength range 3 to 9 µm are in-phase with value  $-\pi/2$ . A sharp  $\pi$ phase shift occurs for H4 at the wavelength of the yield minimum ~9 μm, such that H4 and H6 becomes out-ofphase from 10 to 16 µm. This change of the spectral phase from being in-phase to out-of-phase explains the time-shift of the emissions in Figs. 5(a) and 5(b). At  $\sim$ 16  $\mu$ m, the wavelength corresponding to the yield minimum of H6 in Fig. 3(c), the spectral phase of H6 shifts by  $\pi$ . Additional calculations confirm that the phase shift of the anomalous HHG also occurs around the minima of a laser-intensity scan [63], again validating the robustness of our ab initio results and our semiclassical interpretations. In addition to the emission-time shifts and the sharp spectral-phase shifts being unique characteristics of the anomalous HHG mechanism, they also suggest the potential control of anomalous harmonics by taking advantage of the sign change around the nodes of  $C_s$ .

To conclude, we have characterized the anomalous HHG mechanism in  $MoS_2$ , by development of an *ab initio* methodology that is able to decompose the different contributions to the nonperturbative microscopic current. We have identified different laser-parameter regimes wherein either anomalous or interband currents dominate, thereby resolving a recent debate on the origin of the perpendicular-polarized harmonics in terms of either the anomalous current [10-12,14] or the interband current

[20-24]. We uncovered distinct yield minima at certain field parameters, around which the subcycle emission-time profiles drastically change. Our findings open up the possibility for the experimental generation, identification and time-domain control of pure nonperturbative anomalous currents and high harmonics, which in turn will be invaluable for high-harmonic spectroscopy of Berry curvatures [10,11,14], as such schemes require the generation of pure anomalous harmonics. To provide a direct example, we show in Fig. 4(a) the reconstructed  $\Delta\Omega_z^{\mathbf{k}}$ , employing the harmonic spectrum from Fig. 2(b) in our retrieval algorithm (see Supplemental Material [63]). Our work thus provides a future recipe for the experimental retrieval of Berry curvatures using HHG: (i) identify the anomalous harmonics utilizing their characteristics discussed in this work and (ii) use a reliable retrieval algorithm for reconstruction.

We expect our findings to be general and directly applicable to other materials that have finite Berry curvatures. Indeed, neither the anomalous nor the perpendicular interband harmonics are prohibited by symmetry, and will generally be competing. The presence of minima in the anomalous harmonic yields are also of a general nature, since the amplitudes in Eq. (2) for varying field parameters generally take on both positive and negative values due to the Bessel functions. Finally, all our findings are facilitated by the development of an general ab initio methodology that allows the rigorous decomposition of the currents without the construction of a globally periodic Bloch gauge, which can directly be applied to other complex systems. We expect our approach to be especially useful for ab initio simulations of strong-field interactions in topological insulators such as Chern insulators, where a nonzero Chern number prevents the construction of a globally smooth and periodic Bloch gauge [51,82].

L. Y. and M. B. G. acknowledge support from the National Science Foundation, under Grant No. PHY-2110317, and high performance computational resources provided by the Louisiana Optical Network Infrastructure. L. Y. acknowledges Shicheng Jiang for helpful insights at the initial stage of the project, and thanks Michael Zuerch, Yuki Kobayashi, and Ofer Neufeld for useful discussions.

- \*lun\_yue@msn.com †gaarde@phys.lsu.edu
- [1] R. Karplus and J.M. Luttinger, Hall effect in ferromagnetics, Phys. Rev. **95**, 1154 (1954).
- [2] W. Kohn and J. M. Luttinger, Quantum theory of electrical transport phenomena, Phys. Rev. **108**, 590 (1957).
- [3] E. Adams and E. Blount, Energy bands in the presence of an external force field—II: Anomalous velocities, J. Phys. Chem. Solids **10**, 286 (1959).
- [4] M.-C. Chang and Q. Niu, Berry Phase, Hyperorbits, and the Hofstadter Spectrum, Phys. Rev. Lett. 75, 1348 (1995).

- [5] G. Sundaram and Q. Niu, Wave-packet dynamics in slowly perturbed crystals: Gradient corrections and Berry-phase effects, Phys. Rev. B 59, 14915 (1999).
- [6] D. Xiao, M.-C. Chang, and Q. Niu, Berry phase effects on electronic properties, Rev. Mod. Phys. **82**, 1959 (2010).
- [7] D. Vanderbilt, Berry Phases in Electronic Structure Theory: Electric Polarization, Orbital Magnetization and Topological Insulators (Cambridge University Press, Cambridge, England, 2018).
- [8] T. Brabec and F. Krausz, Intense few-cycle laser fields: Frontiers of nonlinear optics, Rev. Mod. Phys. 72, 545 (2000).
- [9] F. Krausz and M. Ivanov, Attosecond physics, Rev. Mod. Phys. 81, 163 (2009).
- [10] H. Liu, Y. Li, Y. S. You, S. Ghimire, T. F. Heinz, and D. A. Reis, High-harmonic generation from an atomically thin semiconductor, Nat. Phys. **13**, 262 (2017).
- [11] T. T. Luu and H. J. Wörner, Measurement of the Berry curvature of solids using high-harmonic spectroscopy, Nat. Commun. **9**, 916 (2018).
- [12] Y. Bai, F. Fei, S. Wang, N. Li, X. Li, F. Song, R. Li, Z. Xu, and P. Liu, High-harmonic generation from topological surface states, Nat. Phys. 17, 311 (2021).
- [13] C. P. Schmid *et al.*, Tunable non-integer high-harmonic generation in a topological insulator, Nature (London) **593**, 385 (2021).
- [14] Y.-Y. Lv, J. Xu, S. Han, C. Zhang, Y. Han, J. Zhou, S.-H. Yao, X.-P. Liu, M.-H. Lu, H. Weng, Z. Xie, Y. B. Chen, J. Hu, Y.-F. Chen, and S. Zhu, High-harmonic generation in Weyl semimetal β WP<sub>2</sub>crystals, Nat. Commun. 12, 6437 (2021).
- [15] S. Y. Kruchinin, F. Krausz, and V. S. Yakovlev, Colloquium: Strong-field phenomena in periodic systems, Rev. Mod. Phys. **90**, 021002 (2018).
- [16] S. Ghimire and D. A. Reis, High-harmonic generation from solids, Nat. Phys. **15**, 10 (2019).
- [17] J. Li, J. Lu, A. Chew, S. Han, J. Li, Y. Wu, H. Wang, S. Ghimire, and Z. Chang, Attosecond science based on high harmonic generation from gases and solids, Nat. Commun. 11, 2748 (2020).
- [18] E. Goulielmakis and T. Brabec, High harmonic generation in condensed matter, Nat. Photonics **16**, 411 (2022).
- [19] Note that the perpendicular component of the intraband current as defined below is much weaker.
- [20] K. Kaneshima, Y. Shinohara, K. Takeuchi, N. Ishii, K. Imasaka, T. Kaji, S. Ashihara, K. L. Ishikawa, and J. Itatani, Polarization-Resolved Study of High Harmonics from Bulk Semiconductors, Phys. Rev. Lett. 120, 243903 (2018).
- [21] N. Yoshikawa, K. Nagai, K. Uchida, Y. Takaguchi, S. Sasaki, Y. Miyata, and K. Tanaka, Interband resonant high-harmonic generation by valley polarized electron-hole pairs, Nat. Commun. 10, 3709 (2019).
- [22] Y. Kobayashi, C. Heide, H. K. Kelardeh, A. Johnson, F. Liu, T. F. Heinz, D. A. Reis, and S. Ghimire, Polarization flipping of even-order harmonics in monolayer transition-metal dichalcogenides, Ultrafast Sci. 2021, 9820716 (2021).
- [23] J. Cao, F. Li, Y. Bai, P. Liu, and R. Li, Inter-half-cycle spectral interference in high-order harmonic generation from monolayer MoS<sub>2</sub>, Opt. Express **29**, 4830 (2021).
- [24] C. Heide, Y. Kobayashi, A. C. Johnson, F. Liu, T. F. Heinz, D. A. Reis, and S. Ghimire, Probing electron-hole

- coherence in strongly driven 2d materials using high-harmonic generation, Optica 9, 512 (2022).
- [25] R. E. F. Silva, Á. Jiménez-Galán, B. Amorim, O. Smirnova, and M. Ivanov, Topological strong-field physics on sublaser-cycle timescale, Nat. Photonics 13, 849 (2019).
- [26] A. Chacón, D. Kim, W. Zhu, S. P. Kelly, A. Dauphin, E. Pisanty, A. S. Maxwell, A. Picón, M. F. Ciappina, D. E. Kim, C. Ticknor, A. Saxena, and M. Lewenstein, Circular dichroism in higher-order harmonic generation: Heralding topological phases and transitions in Chern insulators, Phys. Rev. B 102, 134115 (2020).
- [27] J. Wilhelm, P. Grössing, A. Seith, J. Crewse, M. Nitsch, L. Weigl, C. Schmid, and F. Evers, Semiconductor Bloch-equations formalism: Derivation and application to high-harmonic generation from dirac fermions, Phys. Rev. B 103, 125419 (2021).
- [28] M. Garg, M. Zhan, T. T. Luu, H. Lakhotia, T. Klostermann, A. Guggenmos, and E. Goulielmakis, Multi-petahertz electronic metrology, Nature (London) 538, 359 (2016).
- [29] M. Garg, H. Y. Kim, and E. Goulielmakis, Ultimate waveform reproducibility of extreme-ultraviolet pulses by highharmonic generation in quartz, Nat. Photonics 12, 291 (2018).
- [30] G. Vampa, T. J. Hammond, N. Thiré, B. E. Schmidt, F. Légaré, C. R. McDonald, T. Brabec, D. D. Klug, and P. B. Corkum, All-Optical Reconstruction of Crystal Band Structure, Phys. Rev. Lett. 115, 193603 (2015).
- [31] G. Vampa, T. J. Hammond, N. Thiré, B. E. Schmidt, F. Légaré, C. R. McDonald, T. Brabec, and P. B. Corkum, Linking high harmonics from gases and solids, Nature (London) 522, 462 (2015).
- [32] Y. Yang, J. Lu, A. Manjavacas, T. S. Luk, H. Liu, K. Kelley, J.-P. Maria, E. L. Runnerstrom, M. B. Sinclair, S. Ghimire, and I. Brener, High-harmonic generation from an epsilonnear-zero material, Nat. Phys. 15, 1022 (2019).
- [33] A. Schiffrin, T. Paasch-Colberg, N. Karpowicz, V. Apalkov, D. Gerster, S. Mühlbrandt, M. Korbman, J. Reichert, M. Schultze, S. Holzner, J. V. Barth, R. Kienberger, R. Ernstorfer, V. S. Yakovlev, M. I. Stockman, and F. Krausz, Optical-field-induced current in dielectrics, Nature (London) 493, 70 (2013).
- [34] M. Schultze, E. M. Bothschafter, A. Sommer, S. Holzner, W. Schweinberger, M. Fiess, M. Hofstetter, R. Kienberger, V. Apalkov, V. S. Yakovlev, M. I. Stockman, and F. Krausz, Controlling dielectrics with the electric field of light, Nature (London) 493, 75 (2013).
- [35] M. Schultze, K. Ramasesha, C. D. Pemmaraju, S. A. Sato, D. Whitmore, A. Gandman, J. S. Prell, L. J. Borja, D. Prendergast, K. Yabana, D. M. Neumark, and S. R. Leone, Attosecond band-gap dynamics in silicon, Science 346, 1348 (2014).
- [36] M. Lucchini, S. A. Sato, A. Ludwig, J. Herrmann, M. Volkov, L. Kasmi, Y. Shinohara, K. Yabana, L. Gallmann, and U. Keller, Attosecond dynamical Franz-Keldysh effect in polycrystalline diamond, Science 353, 916 (2016).
- [37] S. Ghimire, A. D. DiChiara, E. Sistrunk, P. Agostini, L. F. DiMauro, and D. A. Reis, Observation of high-order harmonic generation in a bulk crystal, Nat. Phys. 7, 138 (2011).

- [38] T. T. Luu, M. Garg, S. Y. Kruchinin, A. Moulet, M. T. Hassan, and E. Goulielmakis, Extreme ultraviolet highharmonic spectroscopy of solids, Nature (London) 521, 498 (2015).
- [39] S. Jiang, J. Chen, H. Wei, C. Yu, R. Lu, and C. D. Lin, Role of the Transition Dipole Amplitude and Phase on the Generation of Odd and Even High-Order Harmonics in Crystals, Phys. Rev. Lett. **120**, 253201 (2018).
- [40] H. Lakhotia, H. Y. Kim, M. Zhan, S. Hu, S. Meng, and E. Goulielmakis, Laser picoscopy of valence electrons in solids, Nature (London) 583, 55 (2020).
- [41] A. J. Uzan, G. Orenstein, Á. Jiménez-Galán, C. McDonald, R. E. F. Silva, B. D. Bruner, N. D. Klimkin, V. Blanchet, T. Arusi-Parpar, M. Krüger, A. N. Rubtsov, O. Smirnova, M. Ivanov, B. Yan, T. Brabec, and N. Dudovich, Attosecond spectral singularities in solid-state high-harmonic generation, Nat. Photonics 14, 183 (2020).
- [42] D. Bauer and K. K. Hansen, High-Harmonic Generation in Solids with and Without Topological Edge States, Phys. Rev. Lett. 120, 177401 (2018).
- [43] C. Jürß and D. Bauer, Helicity flip of high-order harmonic photons in haldane nanoribbons, Phys. Rev. A 102, 043105 (2020).
- [44] D. Baykusheva, A. Chacón, J. Lu, T. P. Bailey, J. A. Sobota, H. Soifer, P. S. Kirchmann, C. Rotundu, C. Uher, T. F. Heinz, D. A. Reis, and S. Ghimire, All-optical probe of three-dimensional topological insulators based on highharmonic generation by circularly polarized laser fields, Nano Lett. 21, 8970 (2021).
- [45] N. Tancogne-Dejean, O. D. Mücke, F. X. Kärtner, and A. Rubio, Impact of the Electronic Band Structure in High-Harmonic Generation Spectra of Solids, Phys. Rev. Lett. 118, 087403 (2017).
- [46] R. E. F. Silva, I. V. Blinov, A. N. Rubtsov, O. Smirnova, and M. Ivanov, High-harmonic spectroscopy of ultrafast many-body dynamics in strongly correlated systems, Nat. Photonics 12, 266 (2018).
- [47] T. Hansen, S. V. B. Jensen, and L. B. Madsen, Correlation effects in high-order harmonic generation from finite systems, Phys. Rev. A **105**, 053118 (2022).
- [48] O. Neufeld, N. Tancogne-Dejean, U. De Giovannini, H. Hübener, and A. Rubio, Light-Driven Extremely Nonlinear Bulk Photogalvanic Currents, Phys. Rev. Lett. 127, 126601 (2021).
- [49] K. Nakagawa, H. Hirori, S. A. Sato, H. Tahara, F. Sekiguchi, G. Yumoto, M. Saruyama, R. Sato, T. Teranishi, and Y. Kanemitsu, Size-controlled quantum dots reveal the impact of intraband transitions on high-order harmonic generation in solids, Nat. Phys. 18, 874 (2022).
- [50] R. Resta, Macroscopic polarization in crystalline dielectrics: The geometric phase approach, Rev. Mod. Phys. 66, 899 (1994).
- [51] N. Marzari, A. A. Mostofi, J. R. Yates, I. Souza, and D. Vanderbilt, Maximally localized Wannier functions: Theory and applications, Rev. Mod. Phys. **84**, 1419 (2012).
- [52] R. E. F. Silva, F. Martín, and M. Ivanov, High harmonic generation in crystals using maximally localized Wannier functions, Phys. Rev. B 100, 195201 (2019).
- [53] L. Yue and M. B. Gaarde, Structure gauges and laser gauges for the semiconductor Bloch equations in high-order

- harmonic generation in solids, Phys. Rev. A **101**, 053411 (2020).
- [54] S. Jiang, C. Yu, J. Chen, Y. Huang, R. Lu, and C. D. Lin, Smooth periodic gauge satisfying crystal symmetry and periodicity to study high-harmonic generation in solids, Phys. Rev. B 102, 155201 (2020).
- [55] L. Yue and M. B. Gaarde, Introduction to theory of high-harmonic generation in solids: Tutorial, J. Opt. Soc. Am. B 39, 535 (2022).
- [56] Q. H. Wang, K. Kalantar-Zadeh, A. Kis, J. N. Coleman, and M. S. Strano, Electronics and optoelectronics of two-dimensional transition metal dichalcogenides, Nat. Nanotechnol. 7, 699 (2012).
- [57] K. F. Mak and J. Shan, Photonics and optoelectronics of 2d semiconductor transition metal dichalcogenides, Nat. Photonics 10, 216 (2016).
- [58] S. Manzeli, D. Ovchinnikov, D. Pasquier, O. V. Yazyev, and A. Kis, 2D transition metal dichalcogenides, Nat. Rev. Mater. 2, 17033 (2017).
- [59] P. Giannozzi et al., QUANTUM ESPRESSO: A modular and open-source software project for quantum simulations of materials, J. Phys. Condens. Matter 21, 395502 (2009).
- [60] D. R. Hamann, Optimized norm-conserving Vanderbilt pseudopotentials, Phys. Rev. B **88**, 085117 (2013).
- [61] M. Schlipf and F. Gygi, Optimization algorithm for the generation of ONCV pseudopotentials, Comput. Phys. Commun. 196, 36 (2015).
- [62] J. P. Perdew, K. Burke, and M. Ernzerhof, Generalized Gradient Approximation Made Simple, Phys. Rev. Lett. 77, 3865 (1996).
- [63] See Supplemental Material at http://link.aps.org/ supplemental/10.1103/PhysRevLett.130.166903 for additional details on the propagation method, current decomposition, laser-intensity dependence, and Berry-curvature reconstruction. It includes Refs. [64–66].
- [64] S. Park, N. Mutz, T. Schultz, S. Blumstengel, A. Han, A. Aljarb, L.-J. Li, E. J. W. List-Kratochvil, P. Amsalem, and N. Koch, Direct determination of monolayer MoS<sub>2</sub> and WsE<sub>2</sub> exciton binding energies on insulating and metallic substrates, 2D Mater. 5, 025003 (2018).
- [65] Y. Yu, Y. Yu, Y. Cai, W. Li, A. Gurarslan, H. Peelaers, D. E. Aspnes, C. G. Van de Walle, N. V. Nguyen, Y.-W. Zhang, and L. Cao, Exciton-dominated dielectric function of atomically thin MoS<sub>2</sub> films, Sci. Rep. 5, 16996 (2015).
- [66] W. H. Press, S. A. Teukolsky, W. T. Vetterling, and B. P. Flannery, Numerical Recipes in Fortran 90 the Art of Parallel Scientific Computing (Cambridge University Press, Cambridge, England, 1996).
- [67] E. Blount, Formalisms of band theory, Solid State Phys. 13, 305 (1962).

- [68] C. Aversa and J. E. Sipe, Nonlinear optical susceptibilities of semiconductors: Results with a length-gauge analysis, Phys. Rev. B 52, 14636 (1995).
- [69] J. E. Sipe and A. I. Shkrebtii, Second-order optical response in semiconductors, Phys. Rev. B 61, 5337 (2000).
- [70] M. Gradhand, D. V. Fedorov, F. Pientka, P. Zahn, I. Mertig, and B. L. Györffy, First-principle calculations of the Berry curvature of Bloch states for charge and spin transport of electrons, J. Phys. Condens. Matter 24, 213202 (2012).
- [71] L. H. Thong, C. Ngo, H. T. Duc, X. Song, and T. Meier, Microscopic analysis of high harmonic generation in semiconductors with degenerate bands, Phys. Rev. B 103, 085201 (2021).
- [72] H. K. Avetissian, G. F. Mkrtchian, and K. Z. Hatsagortsyan, Many-body effects for excitonic high-order wave mixing in monolayer transition metal dichalcogenides, Phys. Rev. Res. 2, 023072 (2020).
- [73] H. K. Avetissian, S. S. Israelyan, H. H. Matevosyan, and G. F. Mkrtchian, Saddle-point exciton signature on highorder harmonic generation in two-dimensional hexagonal nanostructures, Phys. Rev. A 105, 063504 (2022).
- [74] G. Vampa, C. R. McDonald, G. Orlando, D. D. Klug, P. B. Corkum, and T. Brabec, Theoretical Analysis of High-Harmonic Generation in Solids, Phys. Rev. Lett. 113, 073901 (2014).
- [75] O. Neufeld, D. Podolsky, and O. Cohen, Floquet group theory and its application to selection rules in harmonic generation, Nat. Commun. 10, 405 (2019).
- [76] D. Baykusheva, A. Chacón, D. Kim, D. E. Kim, D. A. Reis, and S. Ghimire, Strong-field physics in three-dimensional topological insulators, Phys. Rev. A 103, 023101 (2021).
- [77] L. Yue, R. Hollinger, C. B. Uzundal, B. Nebgen, Z. Gan, E. Najafidehaghani, A. George, C. Spielmann, D. Kartashov, A. Turchanin, D. Y. Qiu, M. B. Gaarde, and M. Zuerch, Signatures of Multi-Band Effects in High-Harmonic Generation in Monolayer MoS<sub>2</sub>, Phys. Rev. Lett. 129, 147401 (2022).
- [78] M. Wu, S. Ghimire, D. A. Reis, K. J. Schafer, and M. B. Gaarde, High-harmonic generation from Bloch electrons in solids, Phys. Rev. A 91, 043839 (2015).
- [79] C. Liu, Y. Zheng, Z. Zeng, and R. Li, Polarization-resolved analysis of high-order harmonic generation in monolayer MoS<sub>2</sub>, New J. Phys. **22**, 073046 (2020).
- [80] Y. Lee, D. Kim, D.-E. Kim, and A. Chacón, High harmonic generation in monolayer and bilayer of transition metal dichalcogenide, Symmetry 13, 2403 (2021).
- [81] L. V. Keldysh, Ionization in the field of a strong electromagnetic wave, Sov. Phys. JETP **20**, 1307 (1965).
- [82] T. Thonhauser and D. Vanderbilt, Insulator/Chern-insulator transition in the Haldane model, Phys. Rev. B **74**, 235111 (2006).